Journal of Low Temperature Physics, Vol. 1, No. 4, 1969

Trapped-Ion Motion in Helium II†

William I. Glaberson‡

Department of Physics, University of Oregon
Eugene, Oregon

(Received March 4, 1969)

We present the results of a series of experiments on the mobility of negative ions trapped on quantized vortex lines in superfluid helium. Trapped-ion mobilities were measured as a function of temperature, pressure, and He^3 concentration. Some of the experimental data have been previously reported.[1,2] *The temperature and pressure dependence of trapped-ion mobilities is qualitatively different than that of free ions. The He^3 data strongly suggest that the negative ion bubble does not become deformed on the vortex line. We present a model for a vortex line having a central "core" of normal fluid extending over a distance of several angstroms surrounded by a "tail," a region of excess roton density whose momenta are predominantly aligned opposite to the direction of circulation of the superfluid. This model is used to calculate the drag on a negative ion trapped on a vortex line. The model appears to account for the experimental results satisfactorily.*

1. INTRODUCTION

Quantized vortex lines can be defined as singular lines in superfluid helium about which the circulation is quantized, that is, about which

$$\oint \mathbf{V}_s \cdot ds = l\left(\frac{h}{m}\right) \tag{1}$$

where the $\mathbf{V}_s$ is the superfluid velocity, h is Planck's constant, m is the mass of a helium atom, and l is an integer. We need only be concerned here with singly quantized lines having l equal 1. When a bucket of helium II is set into rotation, solid body rotation, forbidden on quantum-mechanical grounds, is approximated on the average by an almost uniform distribution of vortex lines aligned along the axis of rotation.[3]

Equation (1) is obviously not by itself sufficient to describe all the properties of vortex lines since it leads to unphysically large velocities in the immediate vicinity of the vortex line. In an attempt to understand this critical region better, we have investigated the mobility of negative ions localized along vortex lines as

†Submitted to the Department of Physics of the University of Chicago in partial fulfillment of the requirements for the PhD degree.

‡Present address: Department of Physics, Rutgers · The State University, New Brunswick, New Jersey.

a function of temperature, pressure, and He^3 impurities. These ions are trapped on the lines by virtue of a hydrodynamic potential well they experience in the vicinity of the lines as discussed by Donnelly and Roberts[4] and Parks and Donnelly.[5] Measurements of trapped-ion mobilities were first made by Douglass[6] and Domingo and Donnelly.[7] The mobility μ and transit time τ used throughout this paper are defined by

$$\mu = \frac{v}{E} = \frac{L}{E\tau} \tag{2}$$

where E is the electric field, v is the velocity of the ion, and L is the length of the drift space.

2. EXPERIMENTAL APPARATUS AND TECHNIQUES

The experimental cell and associated electronics are shown in Fig. 1 and a scale drawing of the cell is shown in Fig. 2. There are two regions in the cell, the drift space between G3 and G4 and the storage space between R and G2. These two regions are separated by the gating grids G2 and G3, which are "open" during a pulse and "closed" between pulses. Ions are produced at S by means of an Am^{241} α source of strength 190 μCi and separated by means of a field between S and G1. Negative ions are then pulled towards collector C2 by an appropriate potential. The bottom gating grid G2 is always at a lower (less negative) potential

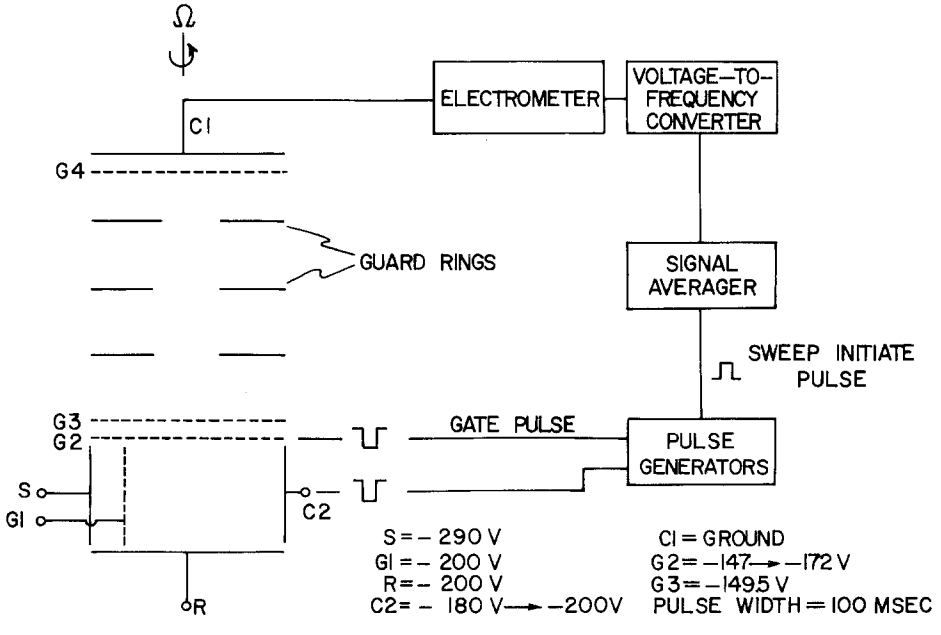

Fig. 1. Schematic diagram of the apparatus for measuring trapped-ion mobilities. The voltage conditions shown were used to obtain most of the data in Figs. 4–7.

than any other electrode in the storage region. Between pulses one has a continuous charge density in the storage region that is cut off sharply at G2. During a pulse, G2 is raised to a potential above G3, thus "opening" the gate. Simultaneously a pulse applied to C2 improves the pulse characteristics by making G1, R, and C2 equipotential, so that all ions are forced through G2. The ions then enter the drift space, and, experiencing the field between G3 and G4, are collected at C1. C1 is shielded from the effects of image charges by means of the Frisch grid G4. The field between G2 and G3 is large, so that the transit time through the gating grid is small. The pulse begins to record as soon as it crosses

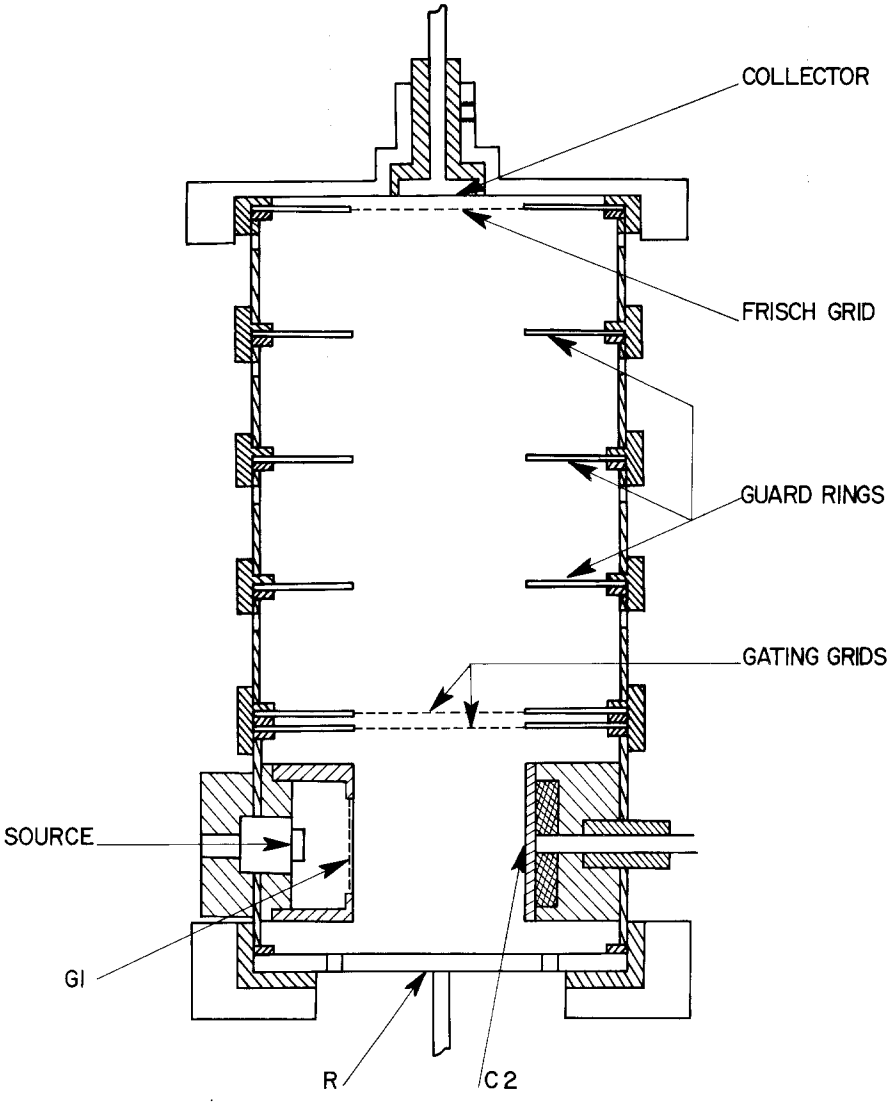

Fig. 2. Scale drawing of the experimental cell.

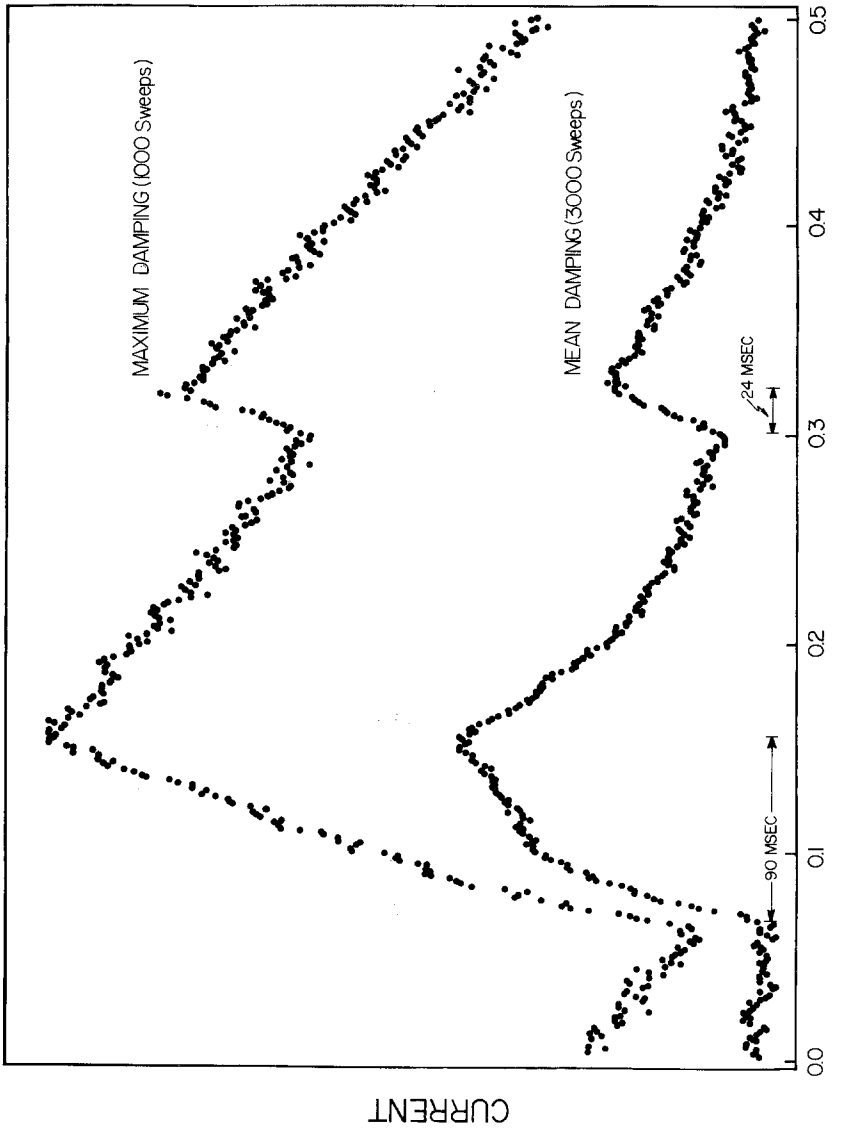

Fig. 3. Output of the signal averager for moderate and maximum damping of the electrometer. Note the relative widths of the free and trapped pulses. The ordinate is arbitrary and corresponds to electrometer current.

G4 and hence transit times are independent of the potential between G4 and C1. Accordingly the drift space is defined as the distance between G3 and G4 and is 4.93 cm. Guard rings on a resistive chain are provided to establish a uniform field in the drift region.

The ion current arriving at C1 is detected with a Keithley model 417 high-speed electrometer whose output is a voltage proportional to the input current. This output is fed into a Hewlett–Packard 2212A voltage-to-frequency converter, and the trains of pulses from it are fed into an RIDL 400-channel analyzer operated in the time–sequence–storage mode. Tektronix 161 pulse generators are used to provide pulses to G2 and C2, while at the same instance providing a trigger pulse to initiate the storage sequence into the analyzer. One storage sequence provides the RIDL memory with the time dependence of the current collected at C1. This process is repeated many times to improve the signal-to-noise ratio.

The pulse technique described above allowed us to detect the time of flight of free and trapped ions simultaneously. Typical examples of the output of the signal averager are shown in Fig. 3 taken with moderate and maximum damping of the electrometer. Another example, at a lower temperature where the ion-trapping cross section has fallen sharply,† is shown in Fig. 4. Since arrival times were independent of damping within experimental resolution, we generally preferred to use maximum damping where possible for reduction of noise.

A series of subsidiary experiments were conducted to find a reliable pulsing technique since, under certain conditions of pulsing, anomalous times of flight could be recorded. Care had to be taken to assure a relatively sharp cutoff of charge density at G2 between pulses. The conditions used in this experiment above 1°K are shown on Fig. 1. A slightly modified pulse technique enhancing the trapped pulse was used below 1°K. One can see from Figs. 3 and 4 that the trapped-ion pulse is considerably narrower than the free-ion pulse, because the potential around G2 forms a well and the trapped ions are constrained on the line and cannot discharge on the grid wires. An investigation of the field dependence of this effect indicated that this bunching introduces negligible uncertainty in the transit time.

The experimental cell is contained in a He^3 refrigerator, which, together with the low-level electronics, is mounted on the University of Oregon 54-in. rotating table. The externally pressurized bearing on this table ensures exceptionally smooth and precise rotations. Speeds up to 60 rpm were used. Electrical communication to and from the rotating system was accomplished by means of mercury slip-rings. The outer helium bath was pumped on through a concentric rotating seal.

The field between S and G1 was varied to accomplish an order-of-magnitude variation of ion current. No effect on free- or trapped-ion transit time was observed, indicating that space-charge effects on the electric field were not important. The angular velocity was varied by almost a factor of 2 with no observable change in transit times, indicating that we are truly dealing with a single vortex line

† This dramatic decrease in ion-trapping cross section at low temperatures was first reported by Tanner.[8]

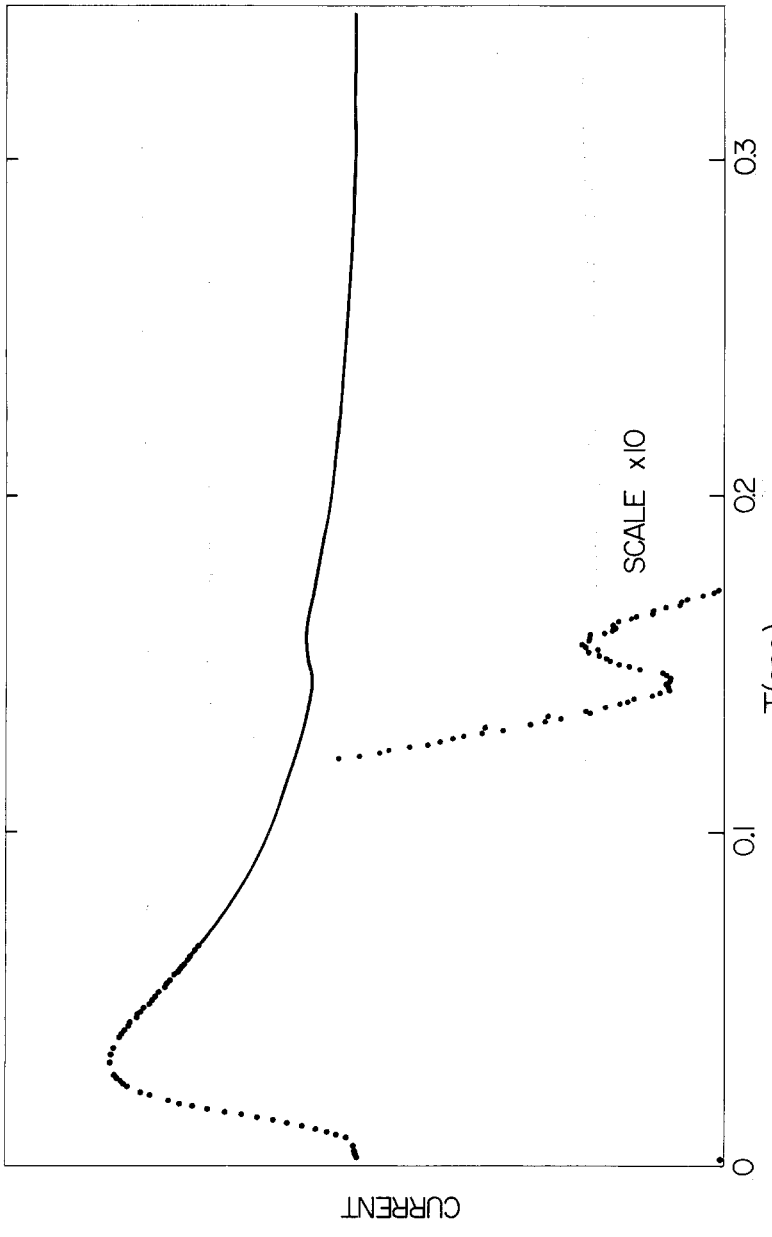

Fig. 4. Output of the signal averager for minimum damping of the electrometer and for a relatively low temperature. Note the small relative amplitude of the trapped-ion pulse.

phenomenon rather than a collective vortex density effect. It was found that we could increase the relative amplitude of the trapped-ion pulse by increasing the time interval between pulses. This enhanced charging of the lines in the storage region had no effect on transit times.

Ion transit times could, in general, be resolved to within a few milliseconds. When the He^3 refrigerator was used, the additional noise introduced by mechanical vibrations necessitated a Krohn–Hite 330B bandpass filter with a high-frequency cut at 100 Hz between the electrometer and the voltage-to-frequency converter. The effect of the filter was calibrated empirically so that overall accuracy of ion transit-time measurement is considered to be better than $\pm 1\%$ plus or minus 2 msec.

Temperatures were measured and regulated using an ac resistance bridge and germanium resistor. The germanium resistor was calibrated against He^4 vapor pressure down to 1.1°K, and was least-squares fitted to a function of the form $R = AT^B e^{c/T}$ on an IBM 360 computer, and extrapolated to 0.7°K. Temperature measurements are considered reliable to 2 mdeg. Pressures were measured with a Heise bourdon gauge and are accurate to 1%.

3. TEMPERATURE DEPENDENCE

Free- and trapped-ion mobilities are shown in Fig. 5 as a function of temperature from 1.7 to 0.69°K. Above 1.7°K, ions are thermally excited out of the vortex lines in times short compared to transit times. Our earlier results[1] have been extended to 0.69°K below which we begin to see vortex-ring-like behavior. Douglass[9] has reported a dramatic increase in escape probability for negative ions at this temperature but offers no explanation for this effect. The free-ion mobilities are in substantial agreement with the mobility data of Reif and Meyer.[10] The curve corresponds approximately to $\exp -\Delta/kT$ with $\Delta/K = 7.97 \pm 0.16$°K compared to Reif and Meyer's value of 8.1°K. Free- and trapped-ion mobilities are nearly independent of electric field having a slight rise, $\sim 10\%$ in both, at low fields. This establishes that in the range 1.7 to 0.7°K trapped-ion motion is a true mobility phenomenon.

Douglass[9] has published measurements at the vapor pressure of trapped-ion mobilities that extend to 0.8°K. His results, which have an accuracy of roughly $\pm 10\%$, are in satisfactory agreement with ours.

4. PRESSURE DEPENDENCE

Free- and trapped-ion mobilities are shown as a function of pressure in Fig. 6 for various temperatures. The application of pressure has two effects: the decrease in the radius of the ion[11,12] and the change in the parameters of the excitation spectrum[13] causing an increase in the roton density. These effects combine for free ions to produce a mobility that first increases and then decreases with increasing pressure with a maximum at about 5 atm. This effect was first observed by Meyer and Reif.[14]

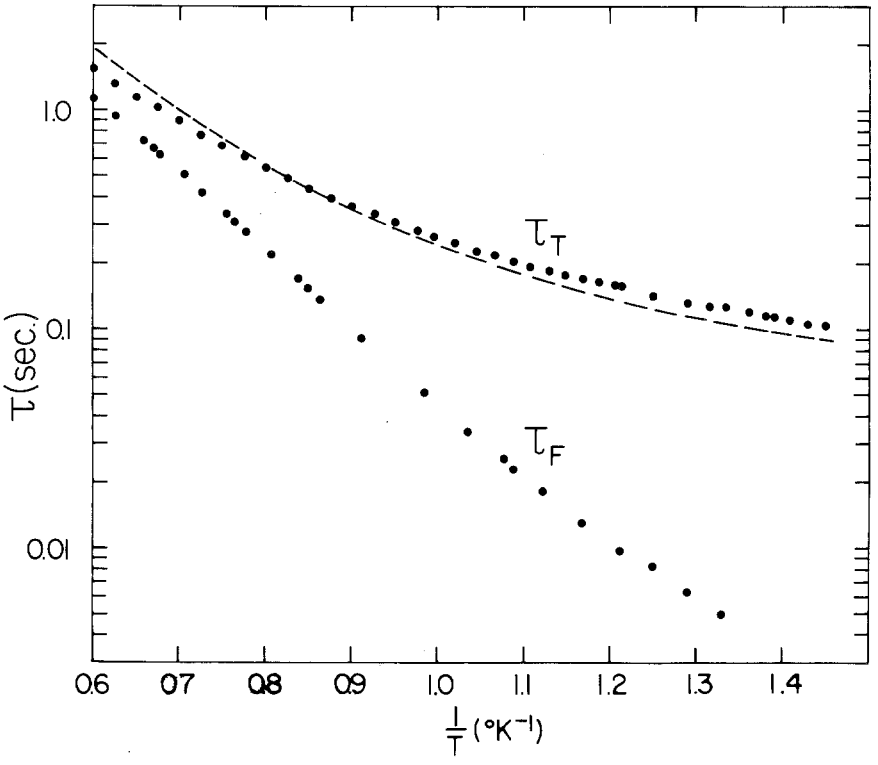

Fig. 5. Temperature dependence of free and trapped-ion transit times at a field of 30 V/cm. The dashed line corresponds to Eq. (23).

Trapped-ion mobilities demonstrate three major qualitative characteristics. First, the effect of a smaller ion radius is to decrease the temperature at which the ion is thermally excited out of the vortex well.[3,9] At a given temperature, then, the ion remains trapped only up to some critical pressures. At 1.6°K this pressure is below 3 atm, while at 1.0°K, the ion remains trapped to within 1% of the freezing pressure. Second, the increase in mobility at low pressures observed for free ions is absent or greatly reduced for trapped ions, indicating that trapped-ion mobilities are probably less sensitive to ion radii. The low-pressure data normalized to zero pressure mobilities are shown on an expanded pressure scale in Fig. 7. Third, the magnitude of the increase in inverse mobility at high pressures is much larger for trapped ions than for free ions. The last two characteristics indicate that the increased transit times experienced by trapped ions cannot be simply a pressure-independent additive retardation.

Additional experimental considerations in the pressure experiments include the use of 30-mil stainless steel capillary tubing between the experimental cell and the room-temperature plumbing (connected in series, of course, with the capillary used customarily in He^3 refrigerators) to minimize heat flux from the helium at the boiling point at the gas–liquid interface, and recalibration of our

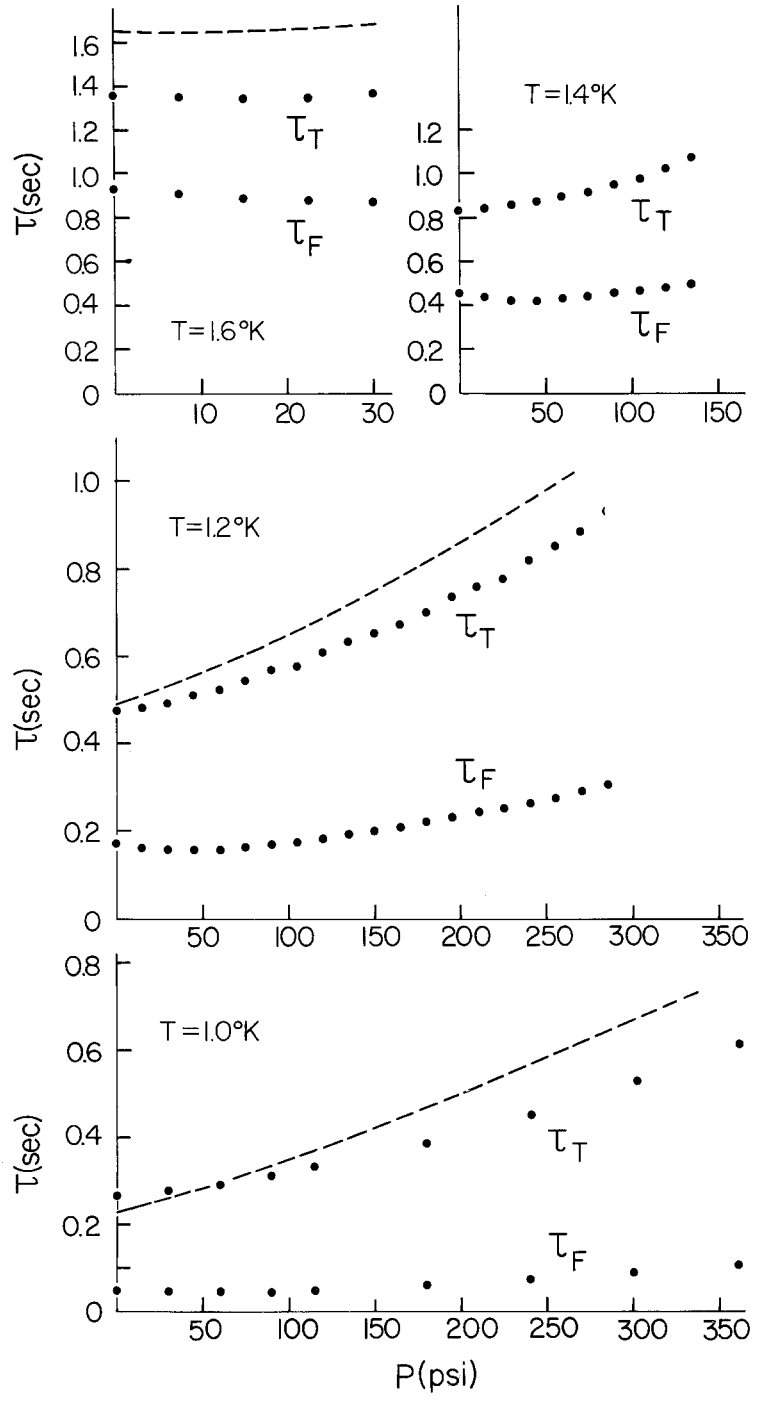

Fig. 6. Pressure dependence of free- and trapped-ion transit times at various temperatures. The dashed line corresponds to Eq. (23).

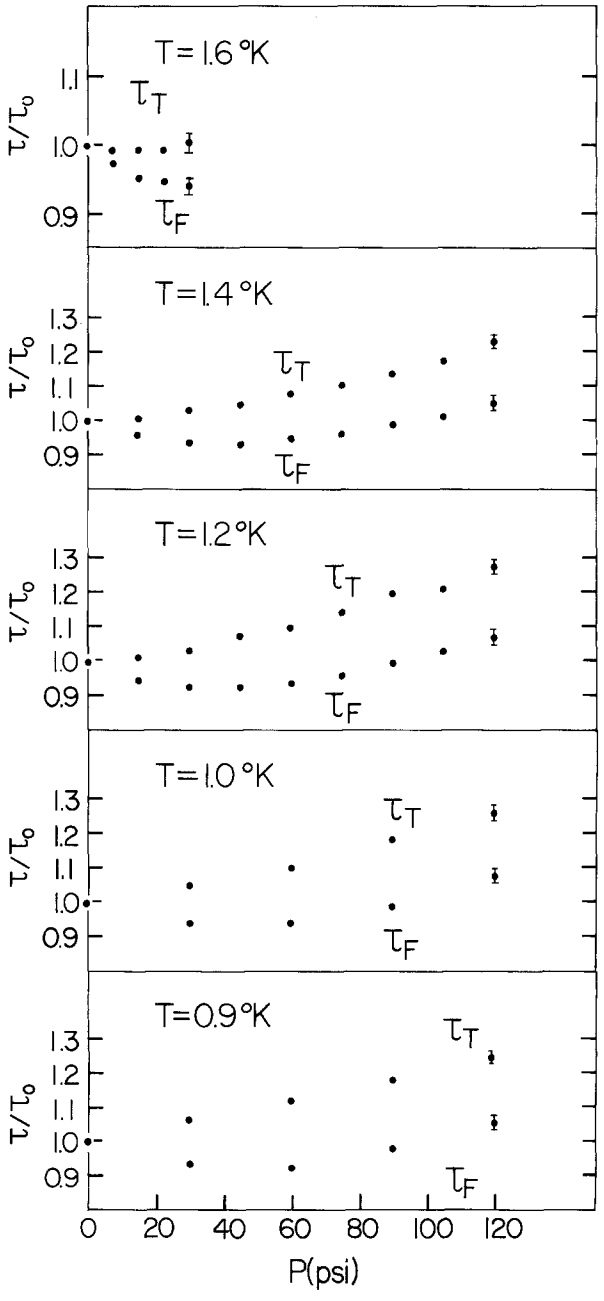

Fig. 7. Pressure dependence of free- and trapped-ion transit times for various temperatures at low pressures. The transit times are plotted relative to their zero pressure values. Note the absence of any initial dip for trapped ions.

germanium resistance thermometer under pressure. The latter consideration proved inconsequential.

5. He^3 IMPURITIES

The effect of He^3 on the mobility of free and trapped ions was investigated for various He^3 concentrations from 0 to 2%. It was found that the excess transit times due to He^3 experienced by the ions were roughly proportional to the He^3 concentration as would be expected for an independent scattering mechanism. The mobility of free and trapped ions in a 2% He^3 solution is shown in Fig. 8. The solid lines are the free- and trapped-ion mobilities in pure He^4 and the dashed lines correspond to mobilities obeying

$$\frac{1}{\mu} = \frac{1}{\mu_4} + 1.73 \tag{3}$$

for both free and trapped ions where μ_4 is the mobility in pure He^4. We can see that to fair accuracy, except perhaps at the highest temperatures, the excess transit time due to the He^3 is temperature-independent and, more important, is the *same* for both free and trapped ions. This implies that, unless there is an excess concentration of He^3 atoms on vortex lines, the ion–He^3 cross section is the same (within $\sim 10\%$) for free and trapped ions. This in turn suggests that the negative ion does not become very deformed when it is trapped on vortex lines.

Additional experimental considerations involve heat-flush problems and thermometry. In the original apparatus the temperature regulator heater was located in the experimental can. It was found that measured mobilities were somewhat dependent on the magnitude of the heater power—the higher the power, the higher the mobility. We interpreted this as a heat-flush effect, the He^3 atoms being driven toward the walls of the can by the normal fluid. Placing the heater in the outer He^4 bath eliminated this problem. Our germanium thermometer was operated in a power-sensitive region so that the presence of He^3 atoms affected the power dissipation, and, hence, the apparent temperature. Recalibration of the thermometer indicated a temperature correction of the order of 5 mdeg for the 2% solution.

6. VORTEX LINE MODEL

We attempt to account for the measured trapped-ion mobilities by recourse to a Landau excitation model applied to the vortex lines. We take excitation–excitation interactions into account and discuss the effect of localization of the excitations on the line. In this discussion we consider only roton excitations since, in the temperature region of interest, mobilities are roton-limited as evidenced by the nearly exponential dependence of free-ion mobilities on temperature. A preliminary discussion of this model has been previously reported.[2]

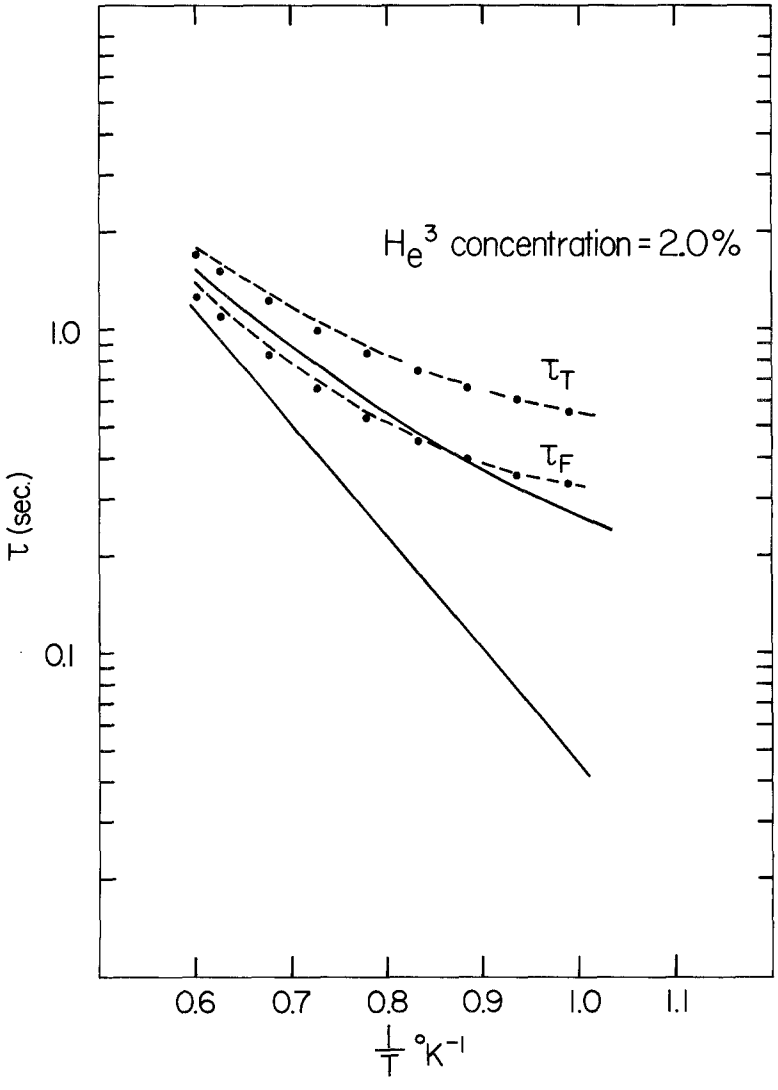

Fig. 8. Temperature dependence of free- and trapped-ion transit times in a 2% He^3 solution. The solid lines correspond to the experimentally determined transit times (in pure He^4) of Fig. 4. The dashed lines correspond to the pure He^4 transit times plus a constant—the same constant for both the free and trapped ions—as given by Eq. (3).

Rotons can be thought of as excitations of the superfluid with an excitation spectrum given by

$$\varepsilon(P) = \Delta + \frac{(P - P_0)^2}{2\mu_0} \tag{4}$$

Consider a gas of rotons having an average velocity $\Delta \mathbf{V}$ with respect to the frame in which the superfluid is at rest and a particular roton in the gas having

momentum **P** in the superfluid rest frame. The energy of this roton as seen from the superfluid frame is $\varepsilon(P)$ (the energy measured in the neutron experiments). The energy of this roton in the roton gas rest frame is then

$$E(P) = \varepsilon(P) - \Delta\mathbf{V} \cdot \mathbf{P} \tag{5}$$

The number of rotons per unit phase space is given by

$$n(P) = \frac{1}{h^3}\{\exp[E(P)/KT] - 1\}^{-1} \tag{6}$$

where the energy in the exponential is the energy as seen from the excitation gas rest frame.[15] We then have

$$n(P) = \frac{1}{h^3}\{e^{\frac{1}{KT}[\varepsilon(P) - \mathbf{P}\cdot(\mathbf{V}_n - \mathbf{V}_s)]} - 1\}^{-1} \tag{7}$$

or, since in our situation the rotons are fixed in the lab (rotating) frame,

$$\begin{aligned} N_r(V, T) &= \int \frac{1}{h^3}\{e^{\frac{1}{KT}\left[\Delta + \frac{(P-P_0)^2}{2\mu_0} + PV\cos\theta\right]} - 1\}^{-1} d^3P \\ &= \frac{2\pi KT}{h^3 V}\int_0^\infty P \ln\left[\frac{1 - e^{-\frac{1}{KT}\left[\Delta + \frac{(P-P_0)^2}{2\mu_0} + PV\right]}}{1 - e^{-\frac{1}{KT}\left[\Delta + \frac{(P-P_0)^2}{2\mu_0} - PV\right]}}\right] dP \end{aligned} \tag{8}$$

where N_r is the number of rotons per unit volume. For small velocities where

$$P_0 V \ll \Delta$$

equation (8) can be approximated by

$$N_r(V, T) = \frac{KT}{P_0 V}\sinh\left(\frac{P_0 V}{KT}\right)\frac{4\pi P_0^2 e^{-\Delta/KT}}{h^3}(2\mu_0 \pi KT)^{1/2} \tag{9}$$

This approximation involves neglecting the 1 in the Bose distribution function of Eq. (8). For large velocities, the approximation is no longer justified and Eq. (8) must be numerically integrated. One obvious feature of the exact integral is the existence of a Landau critical velocity or a velocity where rotons can exist with zero energy—that is, where

$$\left[\Delta + \frac{(P - P_0)^2}{2\mu_0} - PV\right]_{\min} = 0 \tag{10}$$

It is interesting to note that, as the velocity is increased, $N_r(V, T)$ remains finite as the critical velocity is reached although it approaches its "critical" value with infinite slope. The integral reduces asymptotically for $V < V$ critical to

$$N_r(T, V) = \frac{8\pi KT(P_0 + \mu_0 V)}{h^3 V}\left[A - B\tan^{-1}\left(\frac{A}{B}\right)\right] \tag{11}$$

where

$$A = (\mu_0^2 V^2 + 2\mu_0 P_0 V + 2\mu_0 KT - 2\mu_0\Delta)^{1/2}$$

and

$$B = (2\mu_0\Delta - \mu_0^2 V^2 - 2\mu_0 P_0 V)^{1/2}$$

We now consider a calculation of the normal fluid density ρ_n. When $|\mathbf{V}_n - \mathbf{V}_s| = \omega$ is nonzero, the total mass current can be written

$$\mathbf{J} = \rho\mathbf{V}_s + \rho_n(\mathbf{V}_n - \mathbf{V}_s) \tag{12}$$

where the second term is the momentum density associated with the excitations. We then have

$$P_n(\mathbf{V}_n - \mathbf{V}_s) = \int \mathbf{P}\frac{1}{h^3}\{e^{\frac{1}{KT}\left[\Delta + \frac{(P-P_0)^2}{2\mu_0} - \mathbf{P}\cdot(\mathbf{V}_n - \mathbf{V}_s)\right]} - 1\}^{-1} d^3P \tag{13}$$

which for small ω reduces to

$$\rho_n = \frac{P_0^2}{3KT}\frac{4\pi P_0^2 e^{-\Delta/KT}}{h^3}(2\mu_0\pi KT)^{1/2} \tag{14}$$

For large ω, Eq. (12) becomes

$$\rho_n = C + D \tag{15}$$

where

$$C = \frac{2\pi}{\omega h^3}\int_0^\infty \left(\frac{KT}{P\omega}\right)^2 P^3\left[\Delta/KT + \frac{(P-P_0)^2}{2\mu_0 KT}\right]\ln\left\{\frac{1 - e^{-\frac{1}{KT}\left[\Delta + \frac{(P-P_0)^2}{2\mu_0} + P\omega\right]}}{1 - e^{-\frac{1}{KT}\left[\Delta + \frac{(P-P_0)^2}{2\mu_0} - P\omega\right]}}\right\} dP$$

and

$$D = \frac{4\pi K^2}{h^3}(2\mu\pi K)^{1/2}\frac{T^{5/2}}{\omega^3}\sum_{n=1}^{\infty}\frac{1}{u^{3/2}}e^{-\frac{u}{KT}\left(\Delta - \frac{\mu_0\omega^2}{2}\right)}$$

$$\times \sinh\left(\frac{uP_0\omega}{KT}\right)\left[\frac{-P_0}{KT}(\Delta - \tfrac{1}{2}\mu_0\omega^2) - \frac{3P_0}{2n} + \frac{\mu_0 P_0\omega^2}{KT}\right]$$

$$+ \cosh\left(\frac{uP_0\omega}{KT}\right)\left[\frac{P_0^2\omega}{KT} - \frac{\mu_0\omega}{KT}(\Delta - \tfrac{1}{2}\mu_0\omega^2) - \frac{3\mu_0\omega}{2u}\right]$$

C and D are about equal and opposite in sign everywhere except near the critical velocity, where C dominates.

A problem with the above analysis is that the excitation spectrum is assumed independent of the roton density in that, for example, Δ was assumed independent of the velocity. The neutron data of Yarnell *et al.*[16] indicated a Δ that was definitely temperature-dependent, Δ decreasing with increasing temperature. We interpret this temperature dependence as a manifestation of a roton–roton attractive interaction and use an empirical formula of Bendt *et al.*[17]

$$\Delta = \Delta_0 - 0.7383 \times 10^{-37}N \tag{16}$$

to obtain the magnitude of this interaction, at least to first order. We must then solve Eqs. (10) and (16) simultaneously to obtain roton densities. We note at this point that the roton–roton interaction assumed was for completely unpolarized rotons. Near the crticial velocity, the rotons are highly polarized in that the vast majority of them have momentum aligned along a direction close to that of $-\mathbf{V}$.

In the absence of any other assumption, we assume that Eq. (16) applies to these rotons as well. An immediate implication of the roton interaction expression is a rather strongly temperature-dependent critical velocity equal to 58 m/sec at 0.8°K and 37 m/sec at 1.6°K.

The velocity of the superfluid in the vicinity of an isolated vortex line varies inversely with R, the distance from the line. Equations (5) and (7) imply that most of the rotons at small R have energies less than Δ so that they are in effect bound to the vortex line. The statistical mechanics ought properly be applied to the eigenfunctions of the system and not to plane wave rotons whose excitation spectrum was given in Eq. (4). We now attempt to estimate the excitation spectrum for localized roton wave packets.

Rotons, whose density is sought at R, are—on the average— localized to within a distance slightly larger than R from the vortex line, because the average energy of these rotons must be slightly larger than the minimum energy allowed at R. A roton wave packet confined to a dimension of order R must contain a spread in momenta of order h/R by the uncertainty principle. Because of the particular shape of the excitation spectrum, the spread in momentum leads to an increase in energy proportional to $1/R^2$ or more specifically of order

$$\Delta E \approx \frac{\hbar^2}{8\mu_0 R^2} \tag{17}$$

We thus assume a roton excitation spectrum given by

$$\varepsilon(P) = \Delta + \frac{(P - P_0)^2}{2\mu_0} + \frac{\hbar^2}{8\mu_0 R^2} \tag{18}$$

so that equation (8) becomes

$$N_r(T, V) = \frac{2\pi KT}{h^3 V} \int_0^\infty P \ln \left\{ \frac{1 - e^{-\frac{1}{KT}\left[\Delta + \frac{(P-P_0)^2}{2\mu_0} + PV + \frac{\hbar^2}{8\mu_0 R^2}\right]}}{1 - e^{-\frac{1}{KT}\left[\Delta + \frac{(P-P_0)^2}{2\mu_0} - PV + \frac{\hbar^2}{8\mu_0 R^2}\right]}} \right\} dP \tag{19}$$

with a corresponding change for Eq. (15).

Equation (19) has been numerically integrated and solved simultaneously with Eq. (16) by iteration on an IBM 360 computer. The results for various temperatures are shown in Fig. 9 and for various pressures in Fig. 10 plotted as a function of distance from the vortex line. The pressure calculations utilized the variation of the excitation parameters with pressure as inferred from the neutron scattering experiments.[10] The following formulas were used:

$$\begin{aligned} \mu_0 &\to \mu_0 (1.0 - 0.0217\, P) \\ P_0 &\to P_0 (1.0 + 0.0029\, P) \\ \Delta_0 &\to \Delta_0 (1.0 - 0.0075\, P) \end{aligned} \tag{20}$$

where P is the applied pressure in atmospheres and $\mu_0 = 0.16$ M(He^4), $P_0/h = 1.91$ Å^{-1}, and $\Delta_0/K = 8.68$°K. For comparison, the calculation was repeated with the localization term, Eq. (17), deleted; the results are shown in Fig. 11. We can see that the effect of the localization term is to decrease the critical

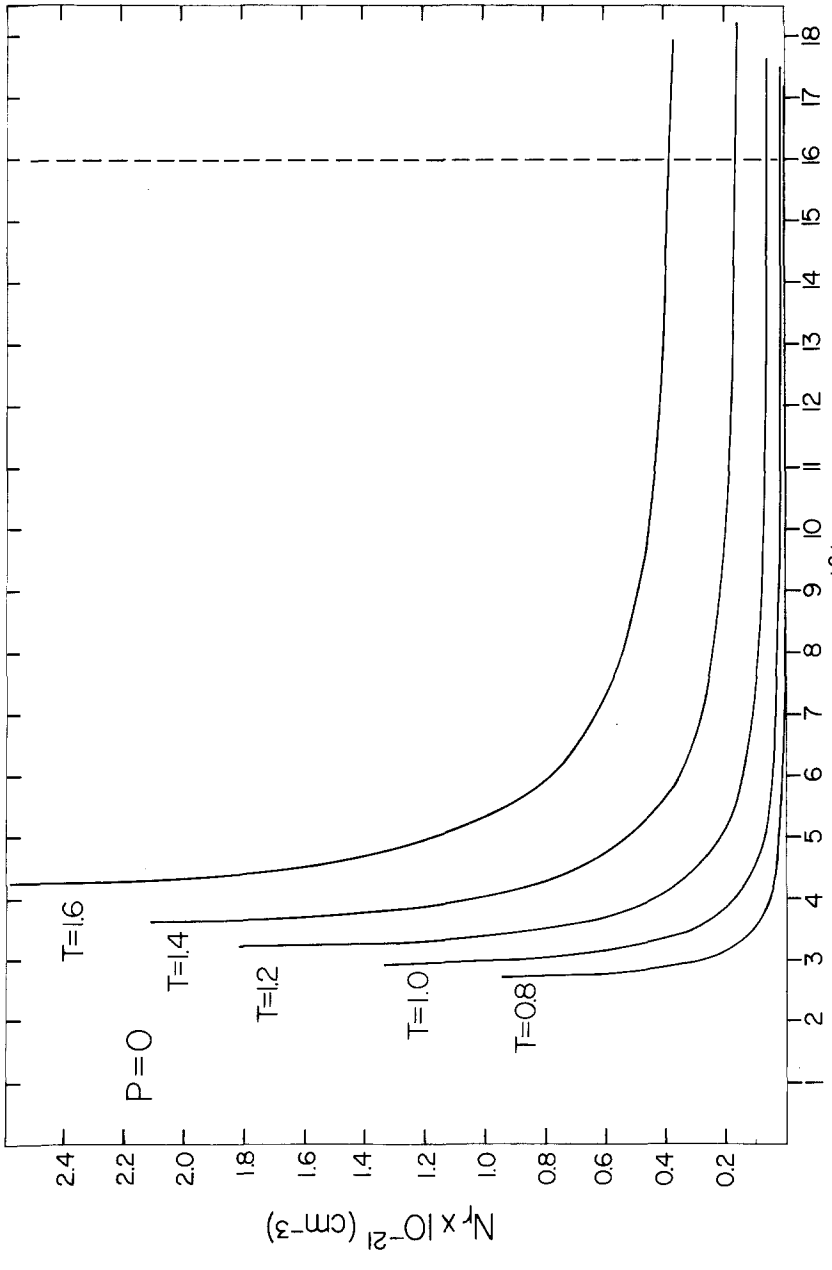

Fig. 9. Roton densities given by Eq. (19) as a function of distance from the vortex line for various temperatures.

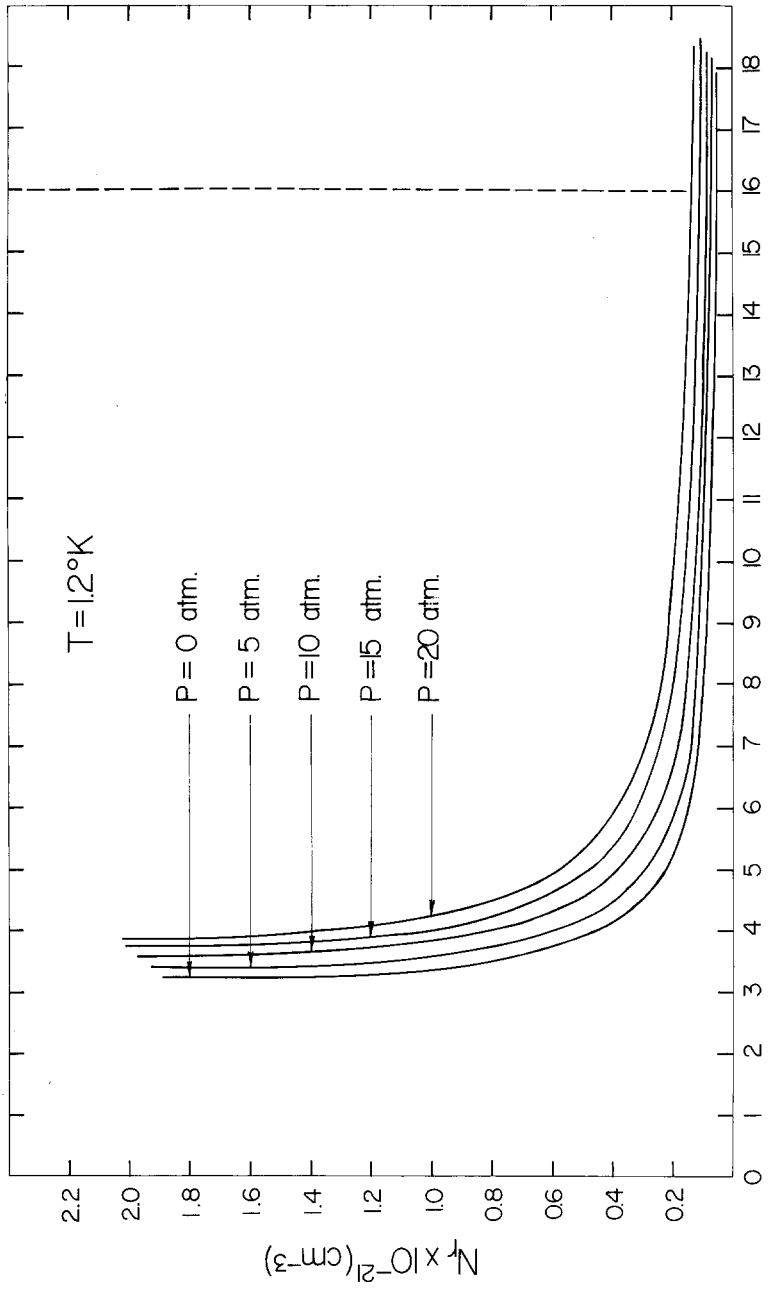

Fig. 10. Roton densities given by Eq. (19) as a function of distance from the vortex line for various pressures at $T = 1.2°K$.

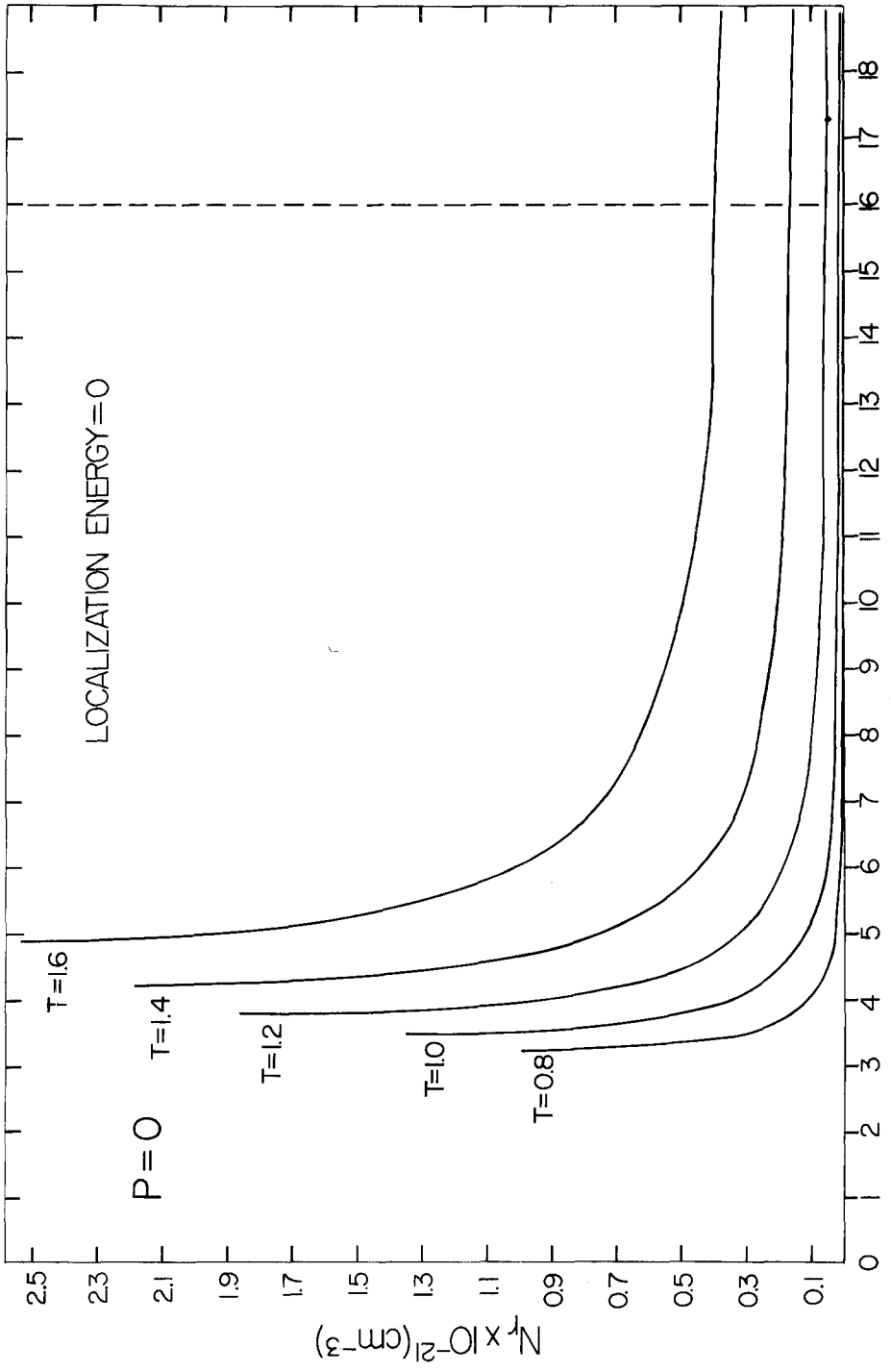

Fig. 11. Roton densities as a function of distance from the vortex line assuming that the localization energy [Eq. (17)] is zero. Note that this figure is almost identical to Fig. 8 except that the critical radii have been displaced to higher values.

radius but otherwise to effect no major qualitative change. Indeed, a justification for incorporating an uncertainty-principle correction to the excitation spectrum is that it has only a small effect on the calculation. The quantity ρ_s/ρ (taken equal to $1 - \rho_n/\rho$), the roton energy gap equal to the minimum value of

$$\left[\Delta + \frac{(P - P_0)^2}{2\mu_0} - PV + \frac{\hbar^2}{8\mu_0 R^2}\right],$$

and the roton density N_r at $T = 1.6°\text{K}$ are shown as a function of R in Fig. 12.

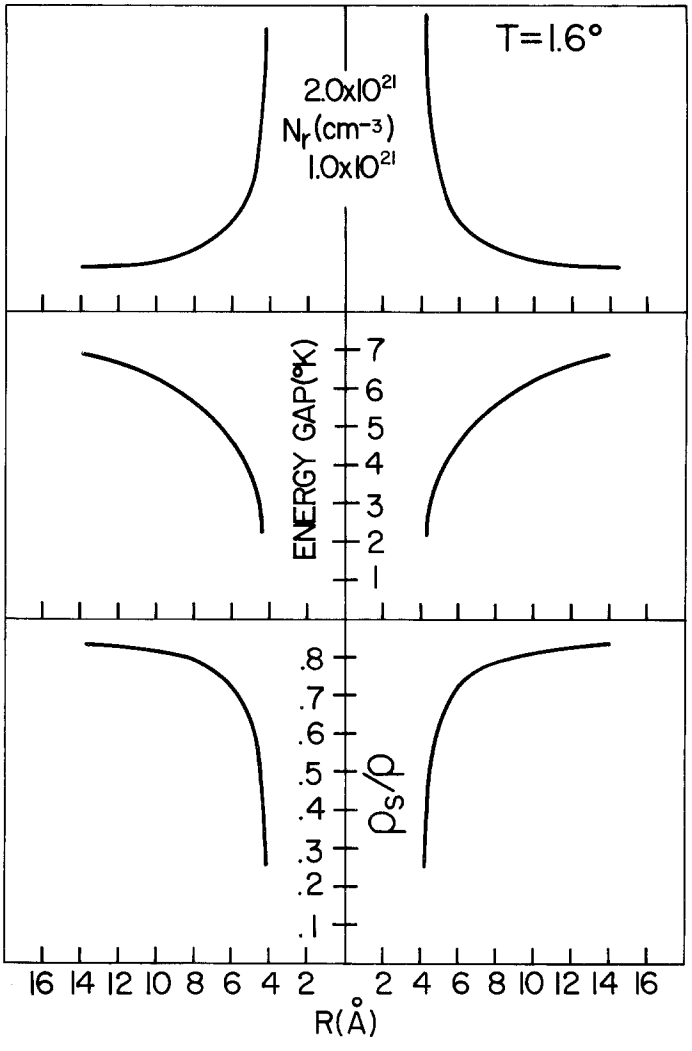

Fig. 12. The variation of various quantities with distance from the vortex time at $T = 1.6°\text{K}$. The upper graph is the roton density reproduced from Fig. 8. The middle graph is the roton energy gap or the minimum value of the quantity $[\Delta + (P - P_0)^2/2\mu_0 - PV + \hbar^2/8\mu_0 R^2]$. The lower graph is the superfluid density fraction ρ_s/ρ taken as $1 - \rho_n/\rho$.

In this model, then, a vortex can be thought of as consisting of two regions: a central normal core whose radius is temperature- and pressure-dependent, and a "tail" in which the roton density (and also ρ_n) increases as the critical radius is approached. The calculation just outlined has a number of problems, some of which were already mentioned. (1) We assumed the roton interaction given by Eq. (16), which may not be valid for polarized rotons. (2) The quasiparticle concept will break down when used to describe particles whose uncertainty of energy due to high collision rates for high densities is of the same order as their energy. (3) The localization energy is uncertain in the absence of roton eigenfunctions. Substantially greater localization energy than we have used will change our results qualitatively. (4) The nature of the core material is not specified; we assume it may be like He I with a density equal to the bulk density. (5) The variation of ρ_s near the core, which was shown in Fig. 11, is least accurately determined. A small amount of superfluid in the core would significantly affect vortex energy calculations. (6) One ought to use the local pressure rather than the applied pressure in determining the Landau excitation spectrum parameters. The Bernoulli pressure at the critical velocity is small compared to the range of pressures considered and was omitted.

7. MOBILITY CALCULATION

We now proceed to calculate negative ion transit times on this model. The trapped ion, whose diameter is the size of the abscissa scales of Figs. 9 to 12, will experience a transit time longer than that of the free ion because of the localized excitations near the vortex line. These break up into two contributions: one due to the core and one due to the tail. The rotons in the tail—except very near the critical radius—comprise a dilute gas and the analysis of Meyer and Reif[14] is expected to be valid. At a given temperature, the drag is then proportional to the number of density of rotons and we can write

$$\tau_{\text{trapped, tail}}(P, T) = \frac{\int_{R_c(P,T)}^{R_i(P)} 2\pi R N_r(P, T, R)\, dR}{\pi R_i^2(P = 0) N_r(P = 0, R = \infty, T)} \tau_{\text{free}}(P = 0, T) \qquad (21)$$

where $R_i(P)$, the ion radius, is taken from Zipfel and Sanders[12] and τ_{free} is determined experimentally.

The above analysis cannot be carried over to the drag induced by the core since the core medium has a high density and behaves "viscously" rather than "molecularly." We compute this viscous effect by assuming that the velocity distribution of the core medium near the surface of the ion in the forward core region is approximately the same as would occur for a sphere moving through an infinite viscous medium. We then proceed with the drag calculation in a manner similar to that of Stokes (see Landau and Lifshitz[18]) but doing the force integral only over the forward core region. We obtain for $R_c \ll R_i$

$$F_{\text{core}} = \tfrac{3}{2}\pi\eta u \frac{R_c^2}{R_i} \qquad (22)$$

where η is the viscosity and u the velocity of the ion. Since this drag force is proportional to the ion velocity, we can write

$$\tau_{\text{trapped}} = \tau_{\text{trapped, tail}} + \tau_{\text{trapped, core}} \tag{23}$$

where

$$\tau_{\text{trapped,core}}(P, T) = \tfrac{3}{2}\pi \frac{L}{e\varepsilon} \frac{R_c^2(P, T)}{R_i(P)} \eta(P, T) \tag{24}$$

and where ε is the electric field and L is the drift length in the experimental cell. We now assume that the thermodynamic properties of the core medium are the same as that of He I were it at temperature T. (The analogue is true, for example, for superconductors when the critical magnetic field is exceeded.) The value of η (at a given bulk density) is then taken from the He I data of Tjerkstra[19] extrapolated to low temperatures with the λ point anomaly ignored.

Equation (23) is shown as the dashed lines in Figs. 5 and 6. There is excellent qualitative agreement and fair quantitative agreement, which is gratifying in an analysis having no adjustable parameters. Note in particular that both the theoretical and experimental trapped ion arrival times exhibit no initial decrease with pressure and exhibit large change from 0 to 25 atm (much larger than the corresponding change for free ions). This last effect can be largely attributed to the strong dependence of η on pressure.

$\tau_{\text{trapped,tail}}$ dominates the drag at high temperatures and low pressures, whereas $\tau_{\text{trapped,core}}$ dominates the drag at low temperatures and high pressures. The range of experimental parameters investigated thus provides a fair test of $\tau_{\text{trapped,core}}$ and $\tau_{\text{trapped,tail}}$ separately.

There are several points that ought to be mentioned with regard to the transit time calculations. One is that the viscous drag was calculated for the velocity field around a hard sphere and not a hollow bubble. It is not clear what boundary conditions apply to a bubble not too much larger than atomic dimensions. Slipping boundary conditions on the bubble would result in a factor of two increase in $\tau_{\text{trapped,core}}$. The second point is that the Meyer and Reif[14] mobility calculation for the free ion utilized a "persistence factor" f related to the probability of a particular roton polarization. The rotons near a vortex line have a higher probability of being polarized perpendicularly to the ion momentum than the rotons encountered by a free ion so that the persistence factor ought to be increased. This would lead to an increase of order but less than 50% in $\tau_{\text{trapped, tail}}$ at the lowest temperature—the effect decreasing with increasing temperature. Another uncertainty, difficult to assess, is introduced into the calculation by the rather long extrapolation of the He I viscosity data.

8. DISCUSSION

The vortex line model discussed in this paper has several important consequences. The calculation of mutual friction[18] depends on the variation of N_r near the vortex line as well as the nature of the vortex core, and should be reconsidered. The excess roton density in the vortex tail and the "He I" of the

vortex core contribute to the entropy of the vortex line and hence will effect vortex ring nucleation models.[21] Roberts and Donnelly[22] have shown that the expressions for the velocity and energy of vortex rings depend on the entropy associated with the vortex line and should be affected. The entropy associated with vortex lines would only negligibly affect the thermodynamics of a quantity of liquid helium. Adiabatically rotating a bucket of helium at 1 mdeg°K to 100 rad/sec would reduce the temperature by about 1%.

Douglass[9] has calculated the drag on the ion owing to vortex waves and shows that this contribution is important only at the lowest temperatures. The data of Fig. 5, which extends to 0.69°K, can be explained without reference to vortex wave drag. Douglass has made some interesting comments on the role of trapped roton states without developing a detailed model.

The problem of the vortex core has been discussed previously from a many-body approach,[23,24] but the present analysis has the attractive feature of explicitly incorporating the observed bulk roton excitation spectrum. There are obviously significant uncertainties in both our vortex model and the transit time calculations. Since the calculation breaks down as the "critical radius" is approached, nothing can be said about the existence of a sharp critical radius. We can, however, say that the excitation density increases markedly near this radius† and it thus represents the scale over which the superfluidity breaks down. In the spirit of these last statements, we believe that our model adequately accounts for our observed trapped ion transit times.

ACKNOWLEDGMENTS

The author wishes to express his appreciation and thanks for the guidance and assistance of Professor Russell J. Donnelly in this research. He also thanks Mr. Donald M. Strayer for invaluable aid in the experimental work; Professors H. E. Hall, W. F. Vinen, and P. H. Roberts for many useful discussions; and Mr. J. V. Radostitz and Mr. W. R. Hackleman for technical and design assistance. This research was supported by the National Science Foundation under Grants NSF-GP-6473 and NSF-GP-6482, and by the Air Force Office of Scientific Research under a Grant AF-AFOSR-785-65. During the course of this research, the author held a Fannie and John Hertz Foundation Fellowship.

REFERENCES

1. W. I. Glaberson, D. M. Strayer, and R. J. Donnelly, *Phys. Rev. Letters* **20**, 1428 (1968).
2. W. I. Glaberson, D. M. Strayer, and R. J. Donnelly, *Phys. Rev. Letters* **21**, 1740 (1968).
3. R. J. Donnelly, W. I. Glaberson, and P. E. Parks, *Experimental Superfluidity* (University of Chicago Press, Chicago, Illinois, 1967).
4. R. J. Donnelly and P. H. Roberts (to be published).
5. P. E. Parks and R. J. Donnelly, *Phys. Rev. Letters* **16**, 45 (1966).

†The critical radius in this model varies approximately as $r_c = 3.2/\sqrt{T_\lambda - T}$ Å. It is interesting to note that Ginsburg and Pitaevskii,[25] using an entirely different approach, obtained a vortex core radius obeying the similar relation $l = 4.0/\sqrt{T_\lambda - T}$ Å.

6. R. L. Douglass, *Phys. Rev. Letters* **13**, 791 (1964).
7. J. J. Domingo and R. J. Donnelly, *Bull. Am. Phys. Soc.* **11**, 479 (1966).
8. D. J. Tanner, *Phys. Rev.* **152**, 121 (1966).
9. R. L. Douglass, *Phys. Rev.* **174**, 255 (1968).
10. F. Reif and L. Meyer, *Phys. Rev.* **119**, 1164 (1960).
11. B. E. Springett, *Phys. Rev.* **155**, 139 (1967).
12. C. Zipfel and T. M. Sanders, Jr., *Proceedings of the Eleventh International Conference on Low Temperature Physics*, to be published; and private communication.
13. D. G. Henshaw and A. D. B. Woods, *Proceedings of the Seventh International Conference on Low Temperature Physics* (University of Toronto Press, Toronto, 1961), p. 539.
14. L. Meyer and F. Reif, *Phys. Rev.* **123**, 727 (1961).
15. R. P. Feynman, *Phys. Rev.* **94**, 262 (1954).
16. J. L. Yarnell, G. P. Arnold, P. J. Bendt, and E. C. Kerr, *Phys. Rev.* **113**, 1379 (1959).
17. P. J. Bendt, R. D. Cowan, and J. L. Yarnell, *Phys. Rev.* **113**, 1386 (1959).
18. L. D. Landau and E. M. Lifshitz, *Fluid Mechanics* (Addison-Wesley Publishing Co., Inc., Reading, Mass., 1959), pp. 67–70.
19. H. H. Tjerkstra, *Physica* **17**, 853 (1952).
20. H. E. Hall, *Phil. Mag. Suppl.* **9**, 89 (1960).
21. S. V. Iordanskii, *Zh. Eksperim. i Teor. Fiz.* **48**, 708 (1965); *Soviet Phys.—JETP* **21**, 467 (1965).
22. H. Roberts and R. J. Donnelly (to be published).
23. E. P. Gross, *Nuovo Cimento* **20**, 454 (1961).
24. A. L. Fetter, *Phys. Rev.* **138**, A709 (1965).
25. V. L. Ginsburg and L. P. Pitaevskii, *Soviet Phys.—JETP* **7**, 858 (1958).